

Article

Arsenic Sulfide Suspended-core Fiber Simulation with Three Parabolic Air Holes for Supercontinuum Generation

Tao Peng ^{1,2,*}, Xunsi Wang ² and Tiefeng Xu ²

¹ College of Electrical Engineering, Zhejiang University of Water Resources and Electric Power, Hangzhou 310018, China

² Laboratory of Infrared Material and Devices, The Research Institute of Advanced Technologies, College of Information Science and Engineering, Ningbo University, Ningbo 315211, China; wangxunsi@nbu.edu.cn (X.W.); xutiefeng@nbu.edu.cn (T.X.)

* Correspondence: pengt@zjweu.edu.cn

Received: 17 May 2020; Accepted: 2 July 2020; Published: 3 July 2020



Abstract: Highly nonlinear suspended-core fibers (SCFs) with tunable dispersion have attracted much attention in the fields of Raman amplification, optical frequency combs, broadband and flat supercontinuum generation (SCG). To address the limitation of applications due to its fragile suspension arms, this study proposes the design of a fiber structure with three parabolic air holes. Numerical simulations are performed to optimize an arsenic sulfide SCF in terms of dispersion management and SCG in the wavelength range from 0.6 μm to 11.6 μm . Results show that the proposed SCF has dual zero-dispersion wavelengths (ZDWs) that can be shifted by adjusting the parabolic coefficient of the air-hole and the equivalent diameter of the suspended core. By means of structural optimization, an SCF with 1 μm equivalent diameter and a parabolic coefficient of 0.18 μm^{-1} is proposed. The first ZDW of the SCF is blue-shifted to 1.541 μm , which makes it possible to use a commercial light source with a cheaper price, more mature technology and smaller volume as the pump source. SCG is studied by solving the generalized nonlinear Schrödinger equation using the split-step Fourier method, and a 0.6–5.0 μm supercontinuum spectrum is obtained at a pump source peak power of 40 kW.

Keywords: suspended-core fiber; parabolic air hole; characteristics analysis; nonlinear optics; supercontinuum

1. Introduction

Because of its wide spectrum, high brightness and high coherence, supercontinuum (SC) has wide applications in photometry, optical coherent imaging, spectroscopy, etc. [1–3]. Supercontinuum generation (SCG) is a kind of spectrum broadening caused by the pump pulse generating new frequency components under the influence of dispersion and various nonlinear effects in medium [4–6]. As a special microstructured fiber, SCF has an important characteristic of adjustable dispersion [7,8]. In addition, it has a smaller core, so a higher nonlinear coefficient can be obtained [9,10]. By optimizing the structure parameters of the SCF, it can obtain a higher nonlinear coefficient and more reasonable dispersion distribution, which is of great help to the SCG.

Silica-based glass has proven to be highly appropriate for the preparation of SCF. Because of the high viscosity, higher pressures are required during the extrusion process, which leads to the deformation of the mold during the drawing process [11]. The nonlinear application of silica-based SCF in the midinfrared region (MIR) is limited due to the infrared cut-off wavelength and lower nonlinear coefficient. In comparison to silica-based glass, the higher optical nonlinearity and broader

transmission window of chalcogenide glass enable the generation of a wider SC spectrum in the MIR [12]. Arsenic sulfide glass is an ideal candidate for the fabrication of SCF, as it has a more mature preparation process, lower loss and better mechanical properties than other chalcogenide glass forms [13,14]. An SC source with a wavelength range from 0.6 μm to 4.1 μm was generated in a 2 cm long three-hole As_2S_3 chalcogenide SCF [15]. Gao et al. demonstrated an SCG spanning a 1.37–5.65 μm wavelength range in a four-hole As_2S_5 chalcogenide SCF [16]. A midinfrared SC spanning the 2.5–5.5 μm spectral region was demonstrated in a 25 mm long three-hole suspended-core As_2S_3 chalcogenide SCF [17]. Xue et al. reported an SC spectrum spanning from 2.05 μm to 6.95 μm , which was generated in a 19-cm long four-hole SCF, which combined a chalcogenide SCF with an As_2S_3 center core [18].

Reducing the core size is among the most effective methods to obtain a higher nonlinear coefficient. At present, there are two types of SCF, as shown in Figure 1. The core part of one type of optical fiber is determined by the suspended-arm. It is only realized by reducing the width of the suspension arm, as shown in Figure 1a, which causes significant difficulty in the preparation of the fiber. The As_2S_3 three-hole SCF proposed by Mouawad et al. [17] and the As_2S_5 four-hole SCF proposed by Gao et al. [19] belong to this kind of SCF. Moreover, various properties of the SCF are significantly affected by breakage of the suspension arm during use. Consequently, another type of SCF structure is proposed to absolve the dependence on the arm. Although the core is no longer determined by the suspension arm, its size cannot be reduced to obtain a larger nonlinear coefficient (Figure 1b), and this structure is more vulnerable than the previous one. The silicate SCF with three holes proposed by Ebendorff-Heidepriem et al. [20] and the As_2S_3 SCF with four holes proposed by Wang et al. [21] are this kind of SCF. Therefore, the design of a more stable structure with lowered dependence of the core on the suspension arm is highly desired [22]. Nevertheless, there are few studies addressing this issue at present.

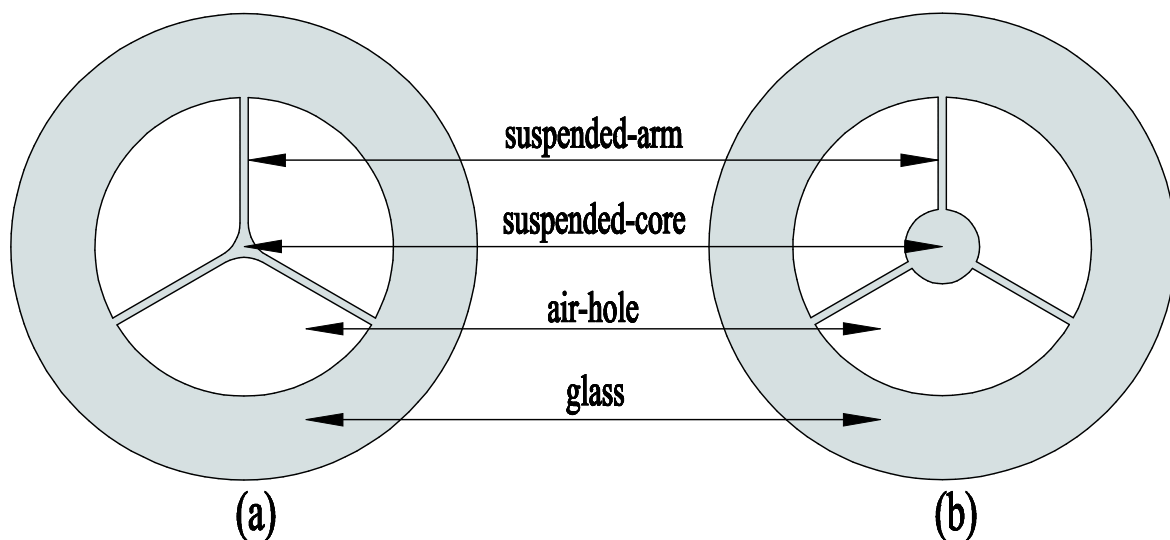


Figure 1. Two different types of suspended-core fibers (SCFs). (a) SCF with non-independent core (b) SCF with independent core.

Moreover, since the zero-dispersion wavelength (ZDW) of the arsenic sulfide bulk glass is $\sim 4 \mu\text{m}$, it will produce a certain blue-shift after being prepared into optical fiber. We present in Table 1 a brief overview of pioneering work in this area. As observed in Table 1, the ZDWs of these fibers are distributed between 2.3 and 4.5 μm due to structural design. However, the pump source in this wavelength range is huge and expensive, which hinders the commercial use of the SC spectrum. The current light source with a wavelength of 1.55 μm has the most mature technology, cheapest price

and smallest volume. If the ZDW of arsenic sulfide SCF is adjusted to this wavelength by structural optimization, the feasibility of the commercial production of SCG devices will be greatly improved.

Table 1. Overview of previously published works.

Year/Ref.	Glass Components	Structure	Length	ZDW	Pump Wavelength	Pump Peak Power	FWHM	Spectral Bandwidth
Unit			cm	μm	μm	kW	fs	μm
2013/[16]	As ₂ S ₃	3-hole	1.3/2.4	2.52	2.6	0.24–1.32	~200	1.520–4.610
2014/[15]	As ₂ S ₃	3-hole	2	2.5	2.5	1.25–4.86	200	0.6–4.1
2014/[23]	As ₂ S ₅	4-hole	4.8	2.28	2.3	0.22–1.55	200	1.370–5.650
2014/[24]	AsSe ₂ -As ₂ S ₅	4-hole	2	3.38	3.389	1.356	~200	1.256–5.400
2016/[17]	As ₂ S ₃	3-hole	2.5	2.65	3.5	0.015	300	2.5–5.5
2018/[24]	As ₂ S ₃ -Ge ₂₀ As ₂₀ Se ₁₅ Te ₄₅	4-hole	19	3.93	4.5	66	150	2.06–6.95

In this paper, an As₂S₃ nonindependent SCF with three parabolic air holes is designed. The effects of the structural parameters of an SCF on its effective refractive index (n_{eff}), nonlinear coefficient, and dispersion can be obtained by simulation. Through optimization of the parameters, the most suitable fiber structure is therefore proposed to produce an SC spectrum. Finally, the generalized nonlinear Schrödinger equation (GNLSE) is adopted in order to obtain the corresponding SC spectrum by adjusting the parameters of the pump source and the SCF, and the basic reasons for its generation are analyzed.

2. Structure Design

Figure 1a,b shows that suspension arms of the SCF are traditionally constructed by the parallel edges of adjacent air holes. Thereby, a smaller core can be obtained by reducing the suspension arm width. In our previous study [25], we found that most of the energy in the fundamental mode (FM) was transmitted in the core; however, a small part leaked to the junction of the arm and core. To obtain a higher nonlinear coefficient, the suspension arm has to be narrowed as much as possible, which makes the preparation of SCF more difficult and significantly reduces the mechanical strength. However, this problem is not solvable by employing a circular air-hole [16,26,27].

In this study, a new type of SCF with a parabolic air-hole is designed. The suspension core is composed of the top of the parabolic air-hole, and the width of the arm can be determined by the parabolic function, instead of by simple parallel lines. The cross-sectional view of the proposed SCF is shown in Figure 2, where the gray shading depicts As₂S₃ glass, and the three white holes depict air. The diameter of the SCF is 125 μm . The inner edge of the air-hole is a parabolic structure, whose specific function is $y = a x^2$, where a is a variable structural parameter, whose value is selected between 0.02 and 0.3 μm^{-1} . When parameter a increases, the top of the air holes becomes narrow, which can make the core smaller. The suspension core is measured by a circle, whose diameter is parameter d [28]. The diameter d determines the size of the suspension core, and it is varied to be 1, 3, 5 and 9 μm . The outer edge of the air-hole is a circular structure with diameter d_1 . In past research, we found that the diameter of the air holes in the SCF has a limited effect on the FM. Hence, d_1 is set to a fixed value of 60 μm , which facilitates the fabrication of the fiber.

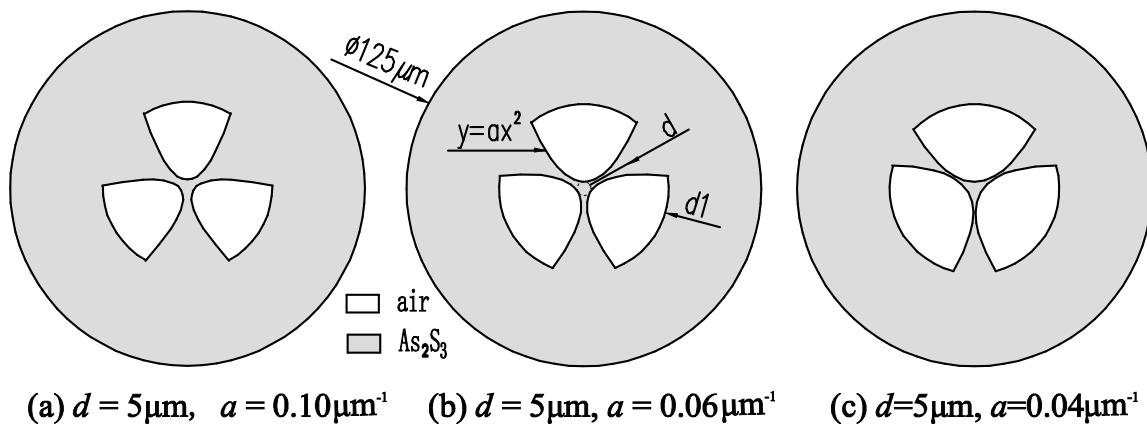


Figure 2. Design views of the SCF geometrical formation.

With the decrease in a , the opening of the air-hole becomes larger, the thickness of the suspension arm becomes thinner and the area of the suspension core decreases, facilitating the binding of the FM in the core. Figure 3a shows the FM field distribution of the structure ($d = 3 \mu\text{m}$, $a = 0.10 \mu\text{m}^{-1}$) at $0.6 \mu\text{m}$ wavelength. The LP_{01} mode with two vertical degenerate modules, indicated with the red arrows in Figure 3b,c is confined tightly in the suspension core demonstrated by the simulation using the commercial software COMSOL.

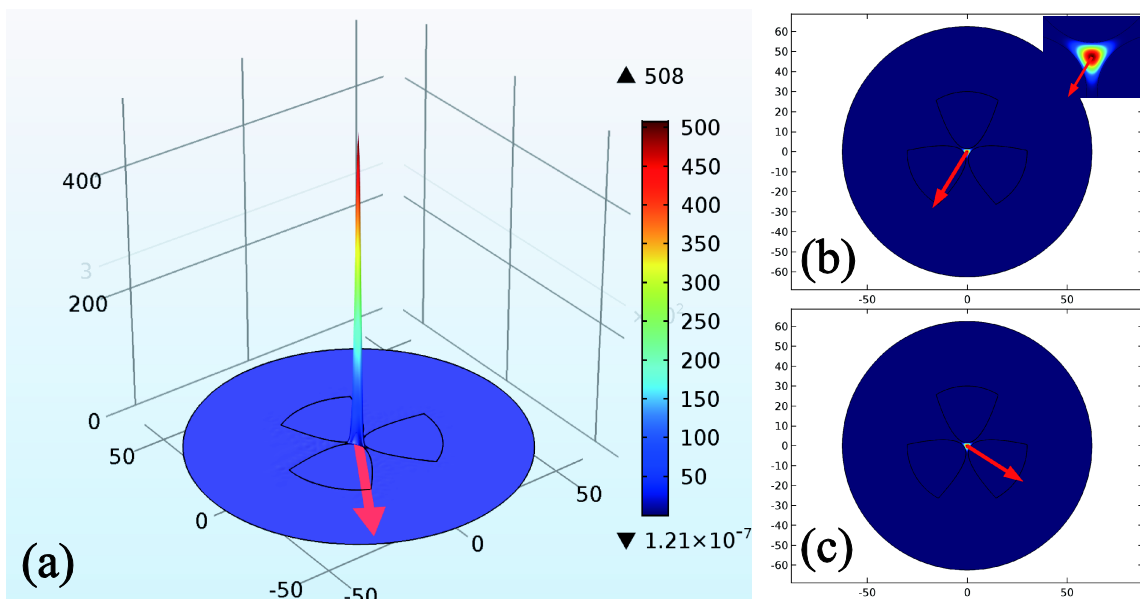


Figure 3. Simulated 3D plot of fundamental mode (FM) (a) and intensity profile of (b) LP_{01-x} and (c) LP_{01-y} ($d = 3 \mu\text{m}$, $a = 0.10 \mu\text{m}^{-1}$, $\lambda = 0.6 \mu\text{m}$).

The shape of parabolic air-hole can be generated by means of extrusion instead of stacking. Owing to the pressure, temperature and deformation of the mold, the shape of the air holes may not be maintained during the hot drawing process, resulting in significant deformation of the edge of the air holes. Figure 4 shows that even if the air-hole has a significant deformation, the distribution of the FM is not affected, as long as the top of the air-hole remains unchanged. Because the propagation mode is not affected by deformation, the n_{eff} of the SCF maintains its original value.

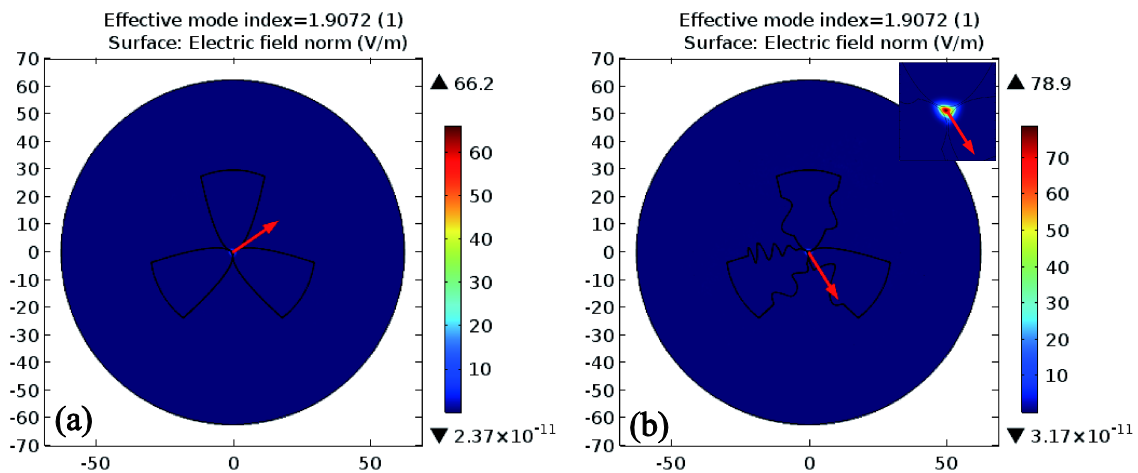


Figure 4. Influence of air-hole ($d = 1 \mu\text{m}$, $a = 0.2 \mu\text{m}^{-1}$) with (a) perfect boundary (b) large defects on SCF's the electric field distribution of FM and n_{eff} .

The traditional suspension arm adopts a parallel structure, which drains part of the energy of the FM, whereas the parabolic structure effectively limits the FM to the core. Assuming that the suspension arm is broken, as shown in Figure 5b,d, the n_{eff} of the parabolic structure does not change, whereas for the traditional structure it decreases from 1.9072 to 1.9067 due to the influence of the propagation mode. Since the nonlinear coefficient, dispersion, and SC spectrum of the fiber are all calculated based on n_{eff} , even a slight variation can cause a dramatic change in these parameters.

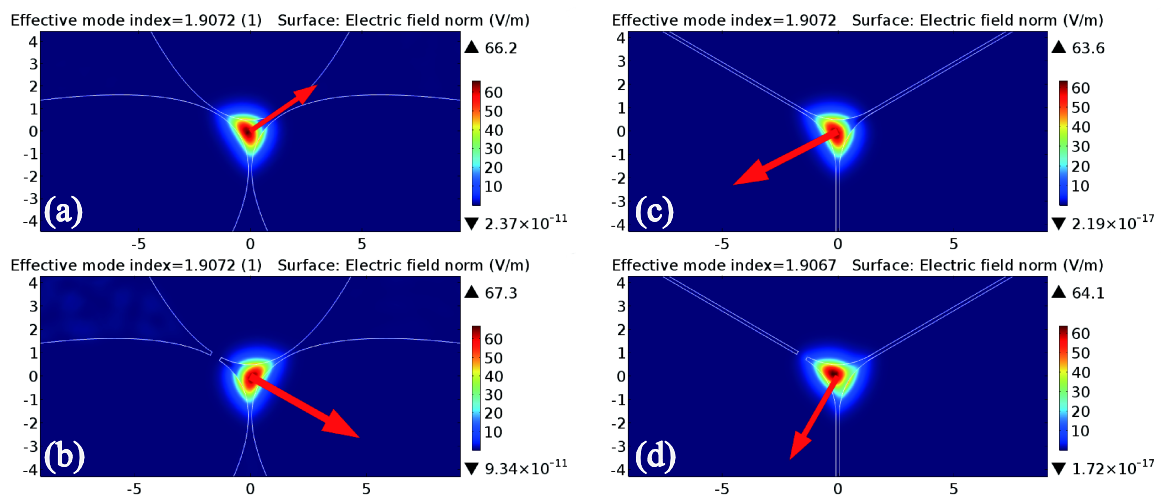


Figure 5. Influence of suspension arm defects on two kinds of SCFs. (a) Proposed SCF without structural defects; (b) proposed SCF with structural defects; (c) traditional SCF without structural defects; (d) traditional SCF with structural defects.

3. Characteristics Analysis

The characteristics of the fiber include the n_{eff} , nonlinear coefficient, dispersion, SC, etc. The study of other characteristics is highly important, such as four-wave mixing (FWM), soliton and the SCG based on these parameters [19]. These characteristics are not the same in block glass and fiber, as they comprise large differences in their various structures of fibers. Hence, it is necessary to study the influence of different structural parameters on the properties of the SCFs.

3.1. Effective Refractive Index

First, we investigate the influence of a on the n_{eff} of the fiber with different d values using COMSOL. The n_{eff} of the fiber is obtained by the refractive index of As_2S_3 , which is calculated by the Sellmeier formula [29]:

$$n^2(\lambda) = 1 + \sum_{i=1}^5 \frac{B_i \lambda^2}{\lambda^2 - C_i'} \quad (1)$$

where B_i and C_i' in (1) are the parameters related to materials. For As_2S_3 block glass, they are 1.8983678, 1.9222979, 0.8765134, 0.1188704, 0.9569903, 0.0225, 0.0625, 0.1225, 0.2025 and 750, respectively. In the simulation, different input wavelengths have different solutions that correspond to different mode fields.

Figure 6a shows the n_{eff} curves as a function of the wavelength at $d = 1 \mu\text{m}$. It can be observed from the figure that the effect of a on the n_{eff} is not particularly apparent, and we found that the function change of the n_{eff} at $d = 3, 5$ and $9 \mu\text{m}$ is basically consistent with the law at $d = 1 \mu\text{m}$; therefore, the introduction of similar data is omitted. We observe that all curves decrease monotonically with the increasing wavelengths, as the fiber structure effectively limits the FM to the suspended core. As shown in Figure 6b, when the value of a is fixed, the n_{eff} of the fiber decreases with the increase of d . Further, this law intensifies with increasing wavelength.

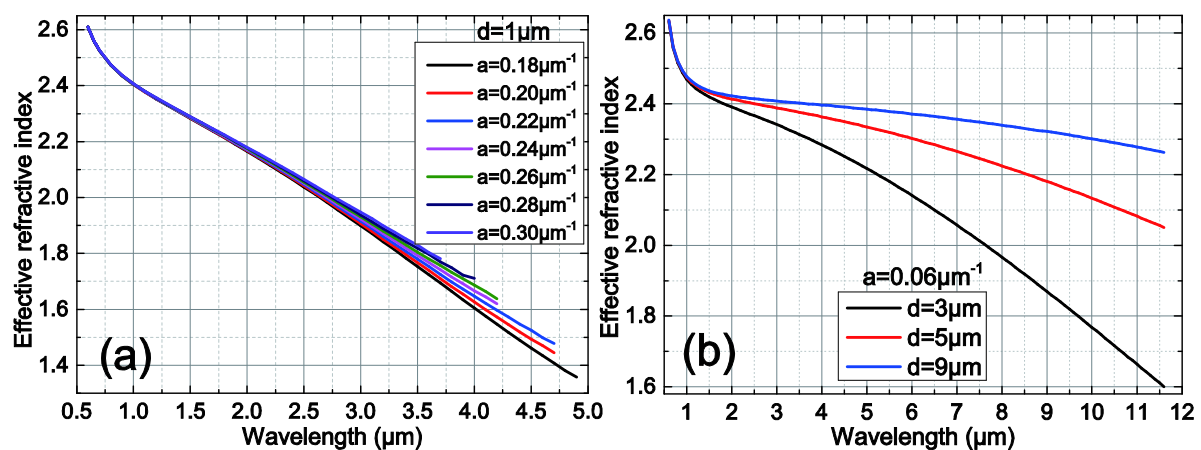


Figure 6. Impact of parameters (a) a , (b) d on n_{eff} of FM.

It is found that with the increase of d , the FM appears at different wavelengths, regardless of a . With the decrease in a and d , the size of the suspension core decreases accordingly. When the operating wavelength is higher than that in the suspended core, the FM can no longer propagate in the core, and there is no corresponding n_{eff} . The simulation indicates that the n_{eff} of the fiber increases with the increase of d . This is because a larger area of the suspended core indicates a greater influence of glass on the FM in comparison to the fiber structure.

Since the n_{eff} is an important aspect of the dispersion calculation and other nonlinear parameters of the SCF, the functional relationship between the n_{eff} and the operating wavelength needs to be accurately determined. In particular, the calculation of SCG is strongly dependent on the dispersion curve, so the fitting effect and fitting error of the function have a great influence on the calculation of these parameters, which makes the selection of fitting function extremely important. However, the traditional difference method has unsatisfactory results in cases where the amount of discrete data is large. A large error arises, particularly in the second derivative. This leads to an inaccuracy in the dispersion value. Numerous types of functions can be employed for fitting. To reduce the systematic error caused by the fitting process, the same function type must be chosen. An excessively low order of the fitting function yields an R-square value that is minuscule, which cannot accurately express the functional relationship. In contrast, if the order of the function is excessively high, although R-square

approaches the value of one, the function generates an extreme value in the second derivation of dispersion, which is not in line with the actual situation of dispersion distribution. Since n_{eff} is based on the Sellmeier formula, we find that the third-order Gaussian function is the most optimal fitting function through fitting comparisons.

$$f(x) = \sum_{i=1}^3 a_i \exp[-(\frac{x - b_i}{c_i})^2] \tag{2}$$

Using the function fitting tool in the MATLAB software, the preliminary function fitting results can be obtained. Because the fitting results given by the software cannot meet the requirements, some parameters need to be adjusted slightly. It is found that fixing other parameters while changing the c_3 value can not only improve the fitting effect, but also ensure that the series of fitting functions have similar change rules. By slightly adjusting c_3 (range-accuracy is 0.0001) in the fitting process, the average R-square and the sum of squares due to error of the fitting function reach values up to 0.999933314 and 8.24×10^{-5} , which can accurately reflect the relationship between the operating wavelength and the n_{eff} .

3.2. Nonlinear Coefficient

The nonlinear coefficient of the fiber is calculated by [30]:

$$\gamma(\lambda) = \frac{2\pi n_2}{\lambda A_{\text{eff}}(\lambda)} \tag{3}$$

where n_2 is the nonlinear refractive index of the fiber material (for As_2S_3 , $n_2 = 2.92 \times 10^{-19} \text{ m}^2/\text{W}$ [31]); λ is the operating wavelength; and $A_{\text{eff}}(\lambda)$ is the effective area of the FM, which can be obtained by the following expression:

$$A_{\text{eff}}(\lambda) = \frac{(\iint_s |E(x, y, \lambda)|^2 dx dy)^2}{\iint_s |E(x, y, \lambda)|^4 dx dy} \tag{4}$$

where $E(x, y, \lambda)$ is the electric field transverse distribution of the FM, which can be determined by simulation. The corresponding $A_{\text{eff}}(\lambda)$ can be obtained after postdata processing.

Equation (3) indicates that three approaches, including the selection of glass with larger n_2 , blue shifting of the operating wavelength and reduction of $A_{\text{eff}}(\lambda)$, are effective in terms of increasing the nonlinear coefficient of the SCF. Because the shape of the air-hole and the diameter of the core are determined by a and d respectively, $A_{\text{eff}}(\lambda)$ and $\gamma(\lambda)$ can be resized by adjusting the two structural parameters.

Figure 7 shows that the nonlinear coefficient of the SCF has a significant inverse proportional relationship with the wavelength. Although the nonlinear coefficient decreases with increasing a , this effect is almost negligible compared to its variation with d . When $\lambda = 0.6 \mu\text{m}$, the maximum nonlinear coefficient can reach $49.26965 \text{ m}^{-1}\text{W}^{-1}$ at $d = 1 \mu\text{m}$, which is more than 70 times of that at $d = 9 \mu\text{m}$. Hence, to obtain a higher nonlinear coefficient, the core should be reduced to the greatest possible degree, which renders the preparation of the SCF more difficult. However, the large loss coefficient of the fiber cannot be ignored due to the limited mode field diameter. Therefore, the operating wavelength should also be considered as another important factor that significantly affects the nonlinear coefficient. From Equation (3) and Figure 7, we can clearly deduce that the operational wavelength is inversely proportional to the nonlinear coefficient. Notably, the absorption peaks of arsenic sulfide glass are mainly concentrated at $\sim 3 \mu\text{m}$ (H_2O) and $\sim 4.3 \mu\text{m}$ (H-S) in the MIR. As there is no obvious absorption peak in the near-infrared region, the loss coefficient of As_2S_3 SCF is not excessively large. The blue-shift of the operating wavelength is another effective approach to improve the nonlinear coefficient.

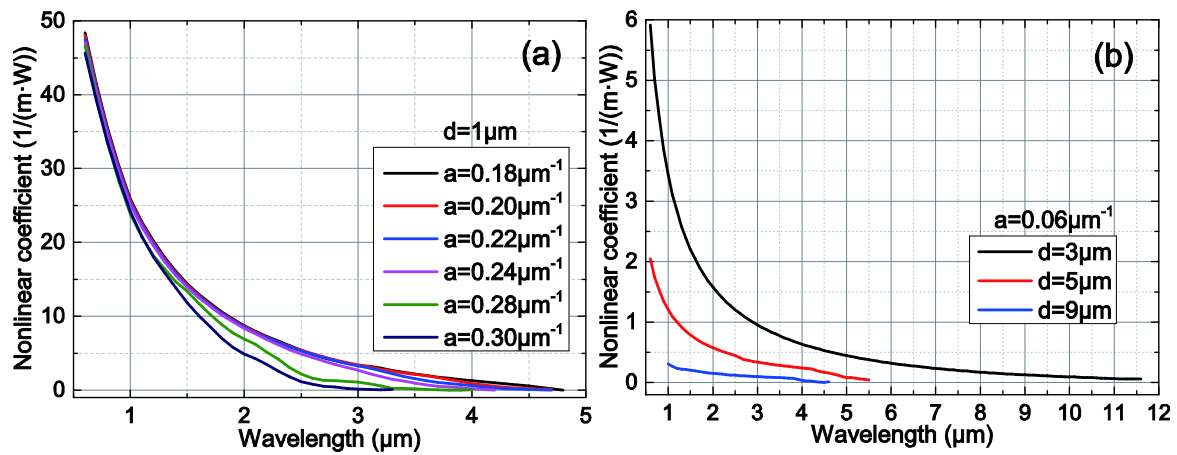


Figure 7. Impact of parameter (a) a , (b) d on the nonlinear coefficient of FM.

3.3. Chromatic Dispersion

Chromatic dispersion in the fiber is predominantly determined by the material and waveguide dispersions. In the case of a large fiber core, chromatic dispersion is mainly determined by material dispersion, whereas waveguide dispersion plays an important role in a narrow core. Due to the small core diameter, the main contribution is waveguide dispersion which can be calculated according to the following equation [32]:

$$D(\lambda) = -\frac{\lambda}{c} \frac{\partial^2 \text{Re}[n_{\text{eff}}(\lambda)]}{\partial \lambda^2} \quad (5)$$

where $\text{Re}[n_{\text{eff}}]$ is the real part of n_{eff} , and c is the velocity of light.

With the decrease in d , it is increasingly difficult for the FM of long wavelengths to transmit within the suspension core. The cut-off wavelength of the FM is red-shifted to 4–5 μm at $d = 1$ μm. Thus, the cut-off wavelength will red-shift further, as d gradually decreases. Simultaneously, with the increase in d , a lower maximum value of dispersion leads to a flatter dispersion curve. This is mainly because the size of the suspended core becomes larger with d , and the n_{eff} of the SCF is therefore increasingly closer to the value of As_2S_3 block glass. The dispersion in the fiber is predominantly determined by the material, such that the dispersion curve and zero-dispersion point (ZDP) are increasingly coincident with the block glass. In contrast, waveguide dispersion plays an important role only when the suspension core is small.

Figure 8a shows the maximum dispersion value of the fiber gradually decreasing from 418.37724 ps/(km·nm) to 154.59883 ps/(km·nm) as a increases from 0.18 to 0.30 μm⁻¹ at $d = 1$ μm, and the wavelength of the maximum red-shifts from 2.481 μm to 2.184 μm. The dispersion curve tends to flatten with increasing d , as shown in Figure 8b, such that the maximum dispersion decreases gradually. Therefore, in order to obtain a wider SC spectrum, it is preferable choosing a fiber structure with a small d . This is mainly because a larger air-hole opening, as shown in Figure 9, when a increases from 0.16 to 0.3 μm⁻¹, leads to more of the light field distribution of the FM overflowing from the suspension arm. This increases the effective mode field area and decreases the nonlinear coefficient. Because the nonlinear coefficient is inversely proportional to the wavelength, as indicated in Equation (3), this is more obvious at long wavelengths. Figure 7 shows that the influence of a on the nonlinear coefficient is not significant, whereas its influence on the dispersion is evident. Figure 8 shows that a has a more significant influence on the dispersion with the decrease in d . Hence, smaller a values lead to higher maximum dispersion values, and a larger slope of dispersion.

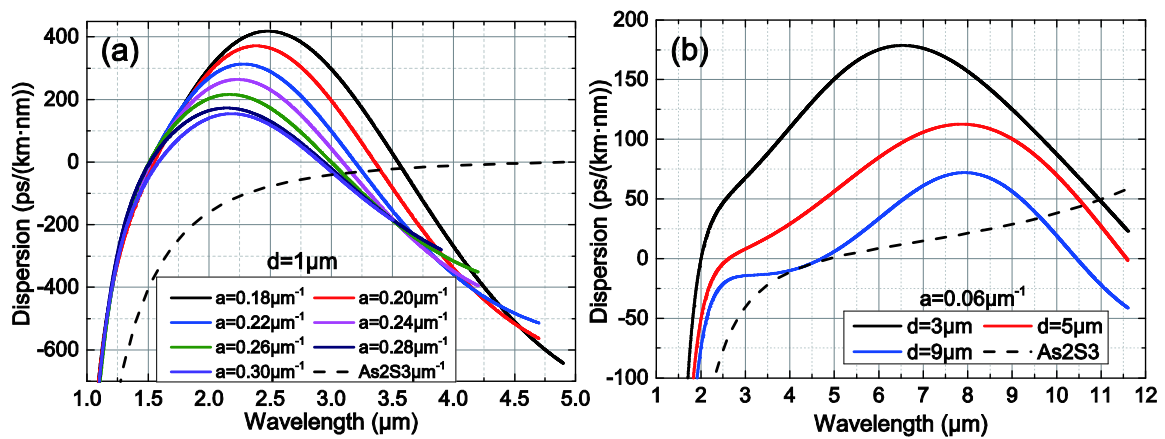


Figure 8. Impact of parameter (a) a , (b) d on the dispersion of FM.

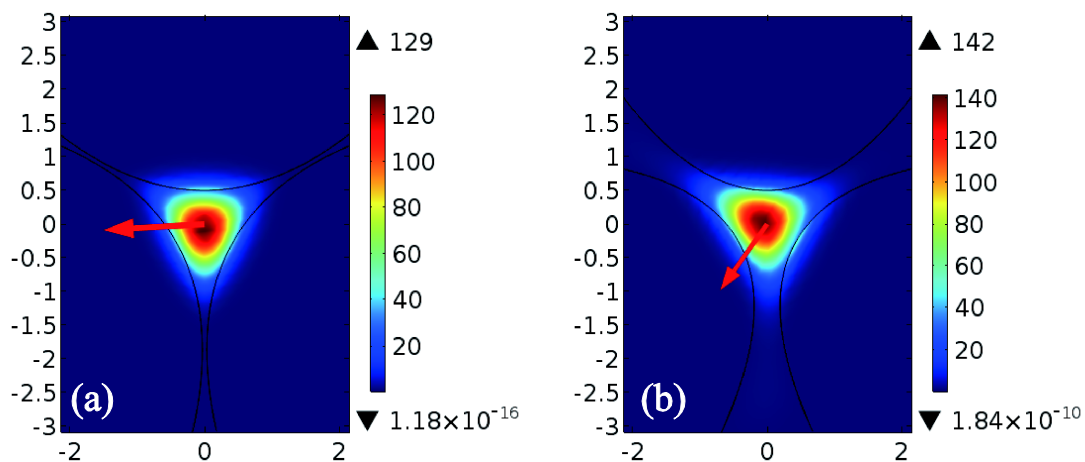


Figure 9. Electric field distribution of FM at $\lambda = 1.5 \mu\text{m}$ for SCFs with $d = 1 \mu\text{m}$ and (a) $a = 0.18 \mu\text{m}^{-1}$, (b) $a = 0.3 \mu\text{m}^{-1}$.

The dispersion of As₂S₃ block glass, as denoted by the black dotted line in Figure 8, is proportional to the wavelength, such that there is only one ZDP of $\sim 4.9 \mu\text{m}$. It was found that almost all the SCFs designed in this study exhibit dual-ZDW when $d \leq 9 \mu\text{m}$. Their first ZDPs are more concentrated, whereas the second ZDPs are more dispersed. Table 2 indicates that the standard deviation is very small, regardless of d . Therefore, parameter a has little influence on the first ZDPs.

Table 2. Mean and standard deviation of first zero-dispersion wavelength (ZDW).

	$d = 1 \mu\text{m}$	$d = 3 \mu\text{m}$	$d = 5 \mu\text{m}$	$d = 9 \mu\text{m}$
Mean (μm)	1.5336	2.0814	2.6860	4.5493
Standard Deviation	0.0243	0.0579	0.0687	0.1218

The influence of a on the second ZDP is more evident. With the increase in a , a clear blue-shift occurs and becomes more significant as d increases. The second ZDP can be blue-shifted from 10.442 to $11.334 \mu\text{m}$ by increasing the value of a when $d = 9 \mu\text{m}$. Furthermore, the diameter d likewise affects the trend of the ZDPs, both of which have the tendency to red-shift as d increases. It was found that the second ZDP has a more obvious red-shift than the first one. The second ZDP red-shifts from ~ 3 to $\sim 11 \mu\text{m}$ as d increases from 1 to $9 \mu\text{m}$.

3.4. Supercontinuum

As a general numerical approach to study SCG, the pulse evolution inside As₂S₃ SCFs was calculated by solving the GNLSE [33]:

$$\frac{\partial A}{\partial z} + \underbrace{\frac{\alpha}{2} A}_{Loss} - \underbrace{\sum_{n \geq 2}^n \beta_n \frac{i^{n+1}}{n!} \frac{\partial^n A}{\partial t^n}}_{Dispersion} = i\gamma \left[\underbrace{|A|^2 A}_{SPM} + \underbrace{\frac{i}{\omega_0} \frac{\partial(|A|^2 A)}{\partial t}}_{SS} - \underbrace{t_R A \frac{\partial |A|^2}{\partial t}}_{SRS} \right] \quad (6)$$

where $A = A(z, t)$ is the electric field envelope of FM; α is the loss coefficient of the SCF, the terms β_n depict various dispersion coefficients in the Taylor series expansion of the propagation constant β at the central frequency ω_0 ; t_R is the Raman response function, which is usually expressed as:

$$t_R = (1 - f_R)\delta(t) + f_R \frac{\tau_1^2 + \tau_2^2}{\tau_1 \tau_2} \exp\left(-\frac{t}{\tau_2}\right) \sin\left(\frac{t}{\tau_1}\right) \quad (7)$$

where the fractional contribution of the delayed Raman response is $f_R = 0.11$ [34], the Raman period is $\tau_1 = 15.5$ fs and the lifetime is $\tau_2 = 230.5$ fs for As₂S₃ [35].

In this study, the split-step Fourier method (SSFM) is employed to calculate the GNLSE. The formula indicates that the dispersion expression on the left has a significant influence on all three nonlinear effects, which are stimulated Raman scattering (SRS), self-steepening (SS) and self-phase modulation (SPM), on the right side of the formula. Therefore, the structural design of the SCF is crucial to obtain a wider SC.

The parameters of the pump source and the structure of the SCF both have a significant influence on SCG. When $d = 1 \mu\text{m}$ and $a = 0.18 \mu\text{m}^{-1}$, the nonlinear coefficient of the fiber is relatively large. More importantly, its first ZDW is $1.541 \mu\text{m}$, which is very close to $1.550 \mu\text{m}$. Presently, the pump source with a $1.550 \mu\text{m}$ wavelength is widely used in communication owing to the maturity of the technology, low cost and high power. As shown in Figure 8a, the second ZDW is $3.543 \mu\text{m}$, and the anomalous dispersion region occurs between the two ZDWs [36]. We fixed the wavelength of the pump source to $1.541 \mu\text{m}$ and the pulse width to 200 fs. SCG is studied by adjusting the pump source peak power. Because of the high nonlinear coefficient of the As₂S₃ material, a short SCF can achieve the saturation of SC, such that its length can be selected as 0.01 m, which can reduce the calculation complexity by omitting the loss factor of the fiber. The nonlinear coefficient of the fiber is $13.84129 \text{ m}^{-1}\text{W}^{-1}$ at $1.541 \mu\text{m}$. Based on the accurate dispersion function obtained in the previous section, the dispersion coefficients β_n are calculated at high accuracy (to improve the accuracy of SC calculation, the tenth-order dispersion coefficient is used in simulation). The specific parameters are shown in Table 3.

Table 3. Values of 1–10 order of dispersion coefficients of SCF with $d = 1 \mu\text{m}$ and $a = 0.18 \mu\text{m}^{-1}$ at $1.541 \mu\text{m}$.

β_1 (fs/mm)	β_2 (fs ² /mm)	β_3 (fs ³ /mm)	β_4 (fs ⁴ /mm)	β_5 (fs ⁵ /mm)	β_6 (fs ⁶ /mm)	β_7 (fs ⁷ /mm)	β_8 (fs ⁸ /mm)	β_9 (fs ⁹ /mm)	β_{10} (fs ¹⁰ /mm)
5.3381×10^5	-6.73833×10^{-16}	1.31008×10^{-27}	-4.6199×10^{-42}	2.39585×10^{-56}	-4.6505×10^{-71}	-2.43177×10^{-85}	5.22843×10^{-99}	5.21097×10^{-112}	$-7.83179 \times 10^{-124}$

Results show that the SCG can be divided into four stages. As shown in Figure 10, the spectrum of the pump source is symmetrically extended to both long and short wavelengths simultaneously by SPM, which results in the basic broadening of the SC. If the SC needs to be extended to the short wavelength, the pump wavelength is of particular importance [37]. The SCF designed in this work adjusts the ZDW to $\sim 1.55 \mu\text{m}$, which can use more common pump sources and extend the SC to $1 \mu\text{m}$.

The spectra show that the broadening width and saturation length of the SC in the early stage is mainly determined by the characteristics of the pump source and optical fiber material. Because of the large nonlinear coefficient of arsenic sulfide glass, as shown in Figure 11a, the fiber only needs to be ~4 mm in length to achieve the saturated output of the SC at $P = 1$ kW. With the increase in peak power, the length is even smaller.

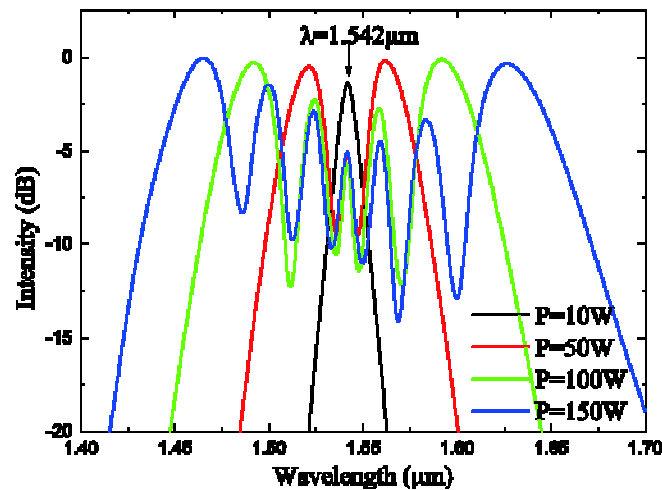


Figure 10. Spectrum spreading at the early stage of supercontinuum generation (SCG) at different peak powers.

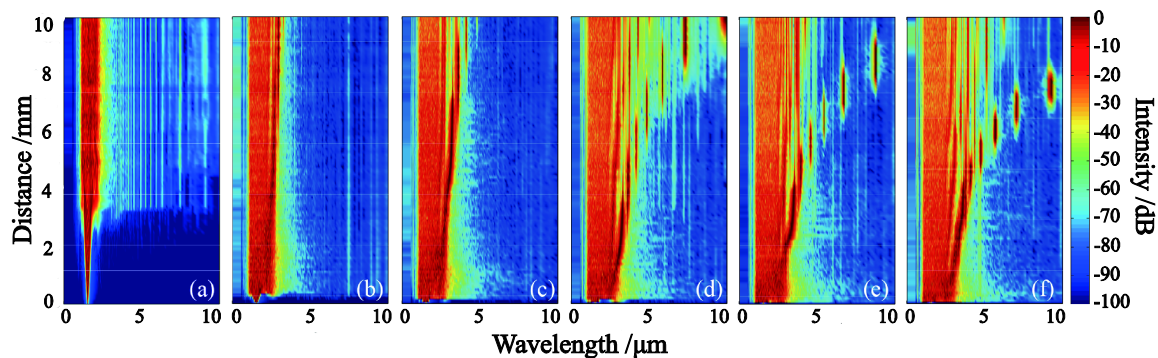


Figure 11. Simulated SCG at peak powers of (a) 1 kW, (b) 10 kW, (c) 20 kW, (d) 30 kW, (e) 40 kW and (f) 50 kW.

In the second stage, the SS effect renders the pulse asymmetric with an increase in the distance or power. This is because when the peak power reaches the Raman threshold, the SRS will selectively increase the spectral width to the long-wavelength measurement, such that the SC exhibits a red-shift [38]. As it can no longer generate frequency components to the short wavelength side, as shown in Figure 11a, the short wavelength will cease to expand after reaching 1 μm at the initial stage.

Subsequently, SC continues to be distorted under the influence of high-order dispersion and nonlinearity of the SCF. Figure 11c shows that when $P = 20$ kW, the higher-order soliton splits into four Raman solitons due to the anomalous dispersion region, and the pulse wavelength of the soliton becomes longer through the soliton self-frequency shift [39]. Moreover, Raman solitons and the dispersive waves emitted by them generate new frequency components through the cross-phase modulation (XPM) and FWM effect, which further broadens the SC.

In the last stage, when the Raman solitons red-shift in the anomalous dispersion region, the dispersive wave quickly fills the energy gap between the solitons. When the wavelength exceeds the second ZDW, the tendency of the spectral red-shift is greatly reduced with the loss of the soliton. Although the dispersive wave and other nonlinear effects can still support the continued broadening of

the SC, the effect will not be obvious. Even with a further increase in the pump energy, the SC cannot continue to red-shift due to saturation [40,41]. Figure 12 shows the evolution of the SC spectrum with increasing pump power (P) from 10 kW to 50 kW. As the peak power reaches 40 kW, the SC will not red-shift after reaching 5.0 μm , which means that the spectrum cannot be extended further. The two ZDPs must not be too far apart, as in that case the energy gap between the solitons cannot be filled by the dispersive wave. Therefore, the fiber structure with two ZDPs, exhibiting flat and low dispersion, is an important factor in the design of ultrawide SC.

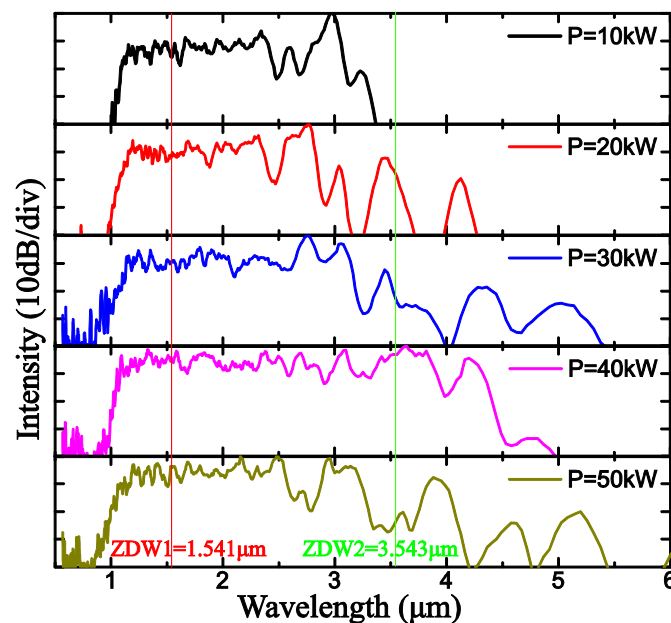


Figure 12. Simulated evolution of SCG pumped at 1.541 μm wavelength at different peak powers.

In addition to the peak power, we also study the influence of pulse duration and the central wavelength of the pump source on the SC spectrum. Figure 13 depicts the evolution of the SC spectrum with increasing pulse duration from 50 fs to 200 fs at peak powers of 40 kW. When the femtosecond pulse width is wider, the soliton number N is larger and the fundamental soliton splits into N higher-order soliton pulses with different red-shifted central frequencies. The closer the split fundamental soliton approaches the second ZDW, the greater the effect of third-order dispersion [42]. At this time, the phase matching is easier to achieve, which enhances the FWM effect. Finally, the spectrum is broadened to the long wavelength by FWM, third-order dispersion, and other nonlinear effects [18]. Moreover, with the increase of the pulse duration, the multi peak oscillation appears in the direction of the long wave, which may be affected by the higher-order dispersion.

When $d = 1 \mu\text{m}$ and $a = 0.18 \mu\text{m}^{-1}$, as shown in Figure 8a, two ZDWs are 1.540 μm and 3.544 μm . We have studied the expansion of the SC spectrum of two near-ZDWs (1.541 μm and 3.543 μm) and their midpoint (2.542 μm) in the anomalous dispersion region. Figure 14 illustrates that the SC spectrum expands in both long and short wave directions with different pump wavelengths. Due to the cut-off of the first ZDW, the pump pulse with the wavelength of 1.541 μm is squeezed by the normal dispersion region, so it is difficult to move to the short wavelength. In the anomalous dispersion region, the dispersive wave makes the band gap between high-order solitons easier to be filled and the SC spectrum red-shifts more easily [43]. Therefore, the ability to extend to the long wavelength is stronger than others, and the spectrum is flatter.

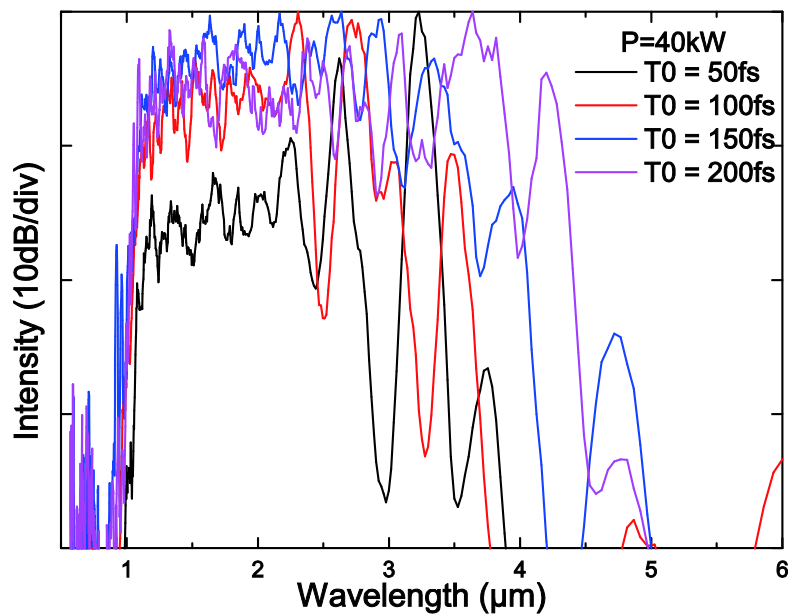


Figure 13. Simulated evolution of SCG pumped at different pulse durations with a pump power of 40 kW.

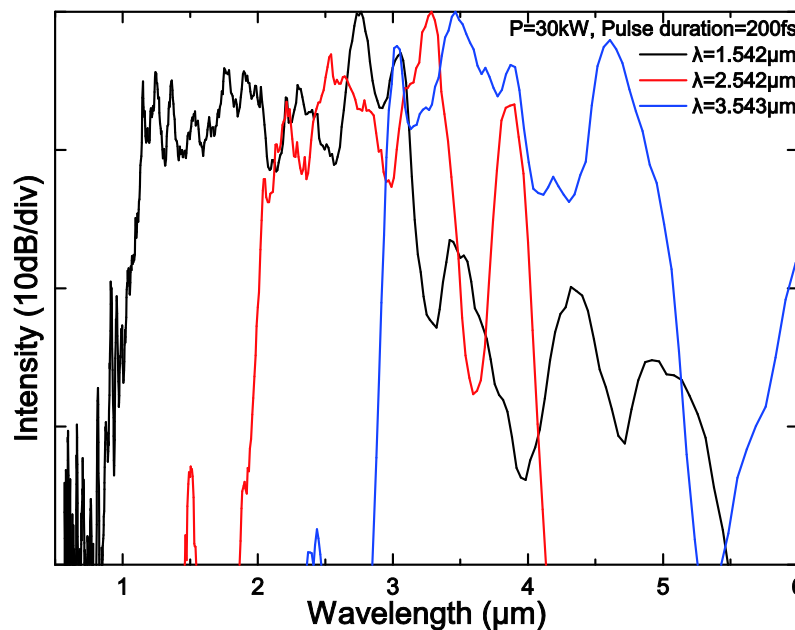


Figure 14. Simulated evolution of SCG with a pump power of 30 kW at different operation wavelengths.

In brief, the peak power and pulse duration of the pump source have a great influence on the red-shift of the SC spectrum, and the central wavelength determines the cut-off of the blue-shift. For the SCF, the dispersion curve can be controlled by adjusting the structural parameters of the fiber, so as to adjust the width and flatness of the SC spectrum.

4. Conclusions

To achieve a smaller core, the traditional SCF must reduce the thickness of its suspension arm, which causes considerable difficulties in the preparation of the SCF and moreover reduces the mechanical strength of the fiber. Because of the fragile suspension arm, the entire SCF is easily damaged during operation. In this study, a special As_2S_3 SCF with three parabolic air holes, allowing for both a

very small core size and a more robust suspension arm, was designed. We carried out a comprehensive analysis of the impact of structural parameters (a and d) on the n_{eff} , nonlinear coefficient, and chromatic dispersion within the wavelength range from 0.6 μm to 11.6 μm using COMSOL.

The simulation results indicate that the two structural parameters are both inversely proportional to the n_{eff} , nonlinear coefficient, and chromatic dispersion. The size of the suspension core is mainly determined by d , which consequently assumes a greater impact than parameter a on the SCF. The higher nonlinear coefficient is mainly achieved by reducing d . By this approach, the maximum dispersion is increased, and the flat dispersion curve is more difficult to obtain. By appropriately increasing parameter a , the nonlinear coefficient is reduced accordingly. However, the flatness of the dispersion curve is significantly improved. The SCF with a flat dispersion and high nonlinear coefficient can be obtained by properly reducing d while increasing a . Moreover, the designed SCFs have dual-ZDWs, both of which red-shift with the increase in d . The second ZDP is likewise affected by a , which in contrast to the trend with d is blue-shifted as a increases. By adjusting a and d , the first ZDP can be red-shifted from 1.509 μm to 4.712 μm , and the second ZDP is 2.909–11.565 μm . In particular, at $d = 1 \mu\text{m}$, the first ZDW is $\sim 1.53 \mu\text{m}$, which enables the generation of the SC by pumping of the SCF by low cost and commercial lasers. According to the dispersion characteristics, the SCF ($d = 1 \mu\text{m}$ and $a = 0.18 \mu\text{m}^{-1}$) can obtain 0.6–5.0 μm SC at the peak power of 40 kW.

Author Contributions: Conceptualization, T.X.; software, T.P.; investigation, T.P.; data curation, T.P.; writing—original draft preparation, T.P.; writing—review and editing, X.W.; visualization, T.P.; supervision, X.W.; project administration, X.W.; funding acquisition, T.X. and X.W. All authors have read and agreed to the published version of the manuscript.

Funding: This research was funded by the National Science Foundation of China under grant number 61875097, 61705091, 61627815, 61775109 and Zhejiang Province Public Welfare Technology Application Research Project under grant number LGF20F010004.

Acknowledgments: The authors gratefully appreciate the support from College of Electrical Engineering, Zhejiang University of Water Resources and Electric Power and Ningbo University that provided office and laboratory.

Conflicts of Interest: The authors declare no conflict of interest. The funders had no role in the design of the study; in the collection, analyses, or interpretation of data; in the writing of the manuscript, or in the decision to publish the results.

References

1. Poudel, C.; Kaminski, C.F. Supercontinuum radiation in fluorescence microscopy and biomedical imaging applications. *J. Opt. Soc. Am. B* **2019**, *36*, A139–A153. [[CrossRef](#)]
2. Kano, H.; Hamaguchi, H.-O. In-vivo multi-nonlinear optical imaging of a living cell using a supercontinuum light source generated from a photonic crystal fiber. *Opt. Express* **2006**, *14*, 2798–2804. [[CrossRef](#)] [[PubMed](#)]
3. Murugkar, S.; Brideau, C.; Ridsdale, A.; Naji, M.; Stys, P.K.; Anis, H. Coherent anti-Stokes Raman scattering microscopy using photonic crystal fiber with two closely lying zero dispersion wavelengths. *Opt. Express* **2007**, *15*, 14028–14037. [[CrossRef](#)] [[PubMed](#)]
4. Monro, T.; Ebendorff-Heidepriem, H.; Schartner, E.; Warren-Smith, S. Sensing in suspended-core optical fibers. *Proc. IEEE Winter Top.* **2011**, 159–160. [[CrossRef](#)]
5. Bravo, M.; Fernández-Vallejo, M.; Echapare, M.; López-Amo, M.; Kobelke, J.; Schuster, K. Multiplexing of six micro-displacement suspended-core Sagnac interferometer sensors with a Raman-Erbium fiber laser. *Opt. Express* **2013**, *21*, 2971–2977. [[CrossRef](#)]
6. Xuan, K.D.; Van, L.C.; Long, V.C.; Dinh, Q.H.; Xuan, L.V.; Trippenbach, M.; Buczynski, R. Dispersion characteristics of a suspended-core optical fiber infiltrated with water. *Appl. Opt.* **2017**, *56*, 1012–1019. [[CrossRef](#)]
7. Russell, P. Photonic crystal fibers. *Science* **2003**, *299*, 358–362. [[CrossRef](#)]
8. Knight, J.C. Photonic crystal fibres. *Nature* **2003**, *424*, 847–851. [[CrossRef](#)]
9. Dong, L.; Thomas, B.K.; Fu, L. Highly nonlinear silica suspended core fibers. *Opt Express* **2008**, *16*, 16423–16430. [[CrossRef](#)]

10. Yakasai, I.; Abas, P.E.; Kaijage, S.F.; Caesarendra, W.; Begum, F. Proposal for a Quad-Elliptical Photonic Crystal Fiber for Terahertz Wave Guidance and Sensing Chemical Warfare Liquids. *Photonics* **2019**, *6*, 78. [[CrossRef](#)]
11. Price, J.H.V.; Monroe, T.M.; Ebendorff-Heidepriem, H.; Poletti, F.; Horak, P.; Finazzi, V.; Leong, J.Y.Y.; Petropoulos, P.; Flanagan, J.C.; Brambilla, G.; et al. Mid-IR Supercontinuum Generation From Nonsilica Microstructured Optical Fibers. *IEEE J. Sel. Top. Quantum Electron.* **2007**, *13*, 738–749. [[CrossRef](#)]
12. Jiao, K.; Yao, J.; Wang, X.-G.; Wang, X.; Zhao, Z.; Zhang, B.; Si, N.; Liu, J.; Shen, X.; Zhang, P.; et al. 1.2–15.2 μm supercontinuum generation in a low-loss chalcogenide fiber pumped at a deep anomalous-dispersion region. *Opt. Lett.* **2019**, *44*, 5545–5548. [[CrossRef](#)]
13. Tao, G.; Ebendorff-Heidepriem, H.; Stolyarov, A.M.; Danto, S.; Badding, J.V.; Fink, Y.; Ballato, J.; Abouraddy, A.F. Infrared fibers. *Adv. Opt. Photonics* **2015**, *7*, 379. [[CrossRef](#)]
14. El-Amraoui, M.; Gadret, G.; Jules, J.C.; Fatome, J.; Fortier, C.; Désévéday, F.; Skripatchev, I.; Messaddeq, Y.; Troles, J.; Brilland, L.; et al. Microstructured chalcogenide optical fibers from As_2S_3 glass: Towards new IR broadband sources. *Opt. Express* **2010**, *18*, 26655–26665. [[CrossRef](#)] [[PubMed](#)]
15. Mouawad, O.; Picot-Clément, J.; Amrani, F.; Strutynski, C.; Smektala, F. 3.5- μm bandwidth mid-infrared supercontinuum generation in a 2-cm long suspended-core chalcogenide fiber. In Proceedings of the Specialty Optical Fibers, Barcelona, Spain, 27–31 July 2014; ISBN 978-1-55752-820-9. [[CrossRef](#)]
16. Gao, W.; El Amraoui, M.; Liao, M.; Kawashima, H.; Duan, Z.; Deng, D.; Cheng, T.; Suzuki, T.; Messaddeq, Y.; Ohishi, Y. Mid-infrared supercontinuum generation in a suspended-core As_2S_3 chalcogenide microstructured optical fiber. *Opt. Express* **2013**, *21*, 9573–9583. [[CrossRef](#)] [[PubMed](#)]
17. Mouawad, O.; Kedenburg, S.; Steinle, T.; Steinmann, A.; Kibler, B.; Désévéday, F.; Gadret, G.; Jules, J.-C.; Giessen, H.; Smektala, F. Experimental long-term survey of mid-infrared supercontinuum source based on As_2S_3 suspended-core fibers. *Appl. Phys. B Lasers Opt.* **2016**, *122*, 177. [[CrossRef](#)]
18. Xue, Z.; Liu, S.; Zhao, Z.; Mi, N.; Wu, B.; Li, X.; Zhang, P.; Wang, X. Infrared Suspended-Core Fiber Fabrication Based on Stacked Chalcogenide Glass Extrusion. *J. Lightwave Technol.* **2018**, *36*, 2416–2421. [[CrossRef](#)]
19. Gao, W.; Duan, Z.; Asano, K.; Cheng, T.; Deng, D.; Matsumoto, M.; Misumi, T.; Suzuki, T.; Ohishi, Y. Mid-infrared supercontinuum generation in a four-hole As_2S_5 chalcogenide microstructured optical fiber. *Appl. Phys. B* **2014**, *116*, 847–853. [[CrossRef](#)]
20. Ebendorff-Heidepriem, H.; Warren-Smith, S.C.; Monroe, T.M. Suspended nanowires: Fabrication, design and characterization of fibers with nanoscale cores. *Opt. Express* **2009**, *17*, 2646–2657. [[CrossRef](#)]
21. Wang, L.; Ma, W.; Zhang, P.; Zhu, L.; Yang, D.; Wang, X.; Dai, S. Mid-Infrared Gas Detection Using a Chalcogenide Suspended-Core Fiber. *J. Lightwave Technol.* **2019**, *37*, 5193–5198. [[CrossRef](#)]
22. Tian, Y.; Zhang, P.; Li, X.; Nie, Q.; Wang, R.; Sun, L.; Chen, P.; Xue, Z.; Wang, X.; Dai, S.; et al. Fabrication and Characterization of Three-hole As_2S_3 Suspended-Core Fibers Based on Robust Extrusion. *IEEE Access* **2018**, *6*, 41093–41098. [[CrossRef](#)]
23. Gao, W.; Duan, Z.; Asano, K.; Cheng, T.; Deng, D.; Matsumoto, M.; Misumi, T.; Suzuki, T.; Ohishi, Y. Supercontinuum Generation in an As_2S_5 Chalcogenide Microstructured Optical Fiber. In Proceedings of the 2014 Conference on Lasers and Electro-Optics (CLEO)-Laser Science to Photonic Applications, San Jose, CA, USA, 8–13 June 2014; IEEE: San Jose, CA, USA, 2014; Volume 116.
24. Cheng, T.; Kanou, Y.; Deng, D.; Xue, X.; Matsumoto, M.; Misumi, T.; Suzuki, T.; Ohishi, Y. Mid-infrared supercontinuum generation in an AsSe_2 - As_2S_5 hybrid microstructured optical fiber. In Proceedings of the 2014 5th International Conference on Optical Communication Systems (OPTICS), Vienna, Austria, 28–30 August 2014; pp. 1–6.
25. Peng, T.; Xu, T.; Wang, X. Simulation Study on Dispersion Properties of As_2S_3 Three-Bridge Suspended-Core Fiber. *IEEE Access* **2017**, *5*, 17240–17245. [[CrossRef](#)]
26. Duhant, M.; Renard, W.; Canat, G.; Nguyen, T.N.; Smektala, F.; Troles, J.; Coulombier, Q.; Toupin, P.; Brilland, L.; Bourdon, P.; et al. Fourth-order cascaded Raman shift in AsSe chalcogenide suspended-core fiber pumped at 2 μm . *Opt. Lett.* **2011**, *36*, 2859. [[CrossRef](#)]
27. Anashkina, E.A.; Shiryaev, V.S.; Koptev, M.Y.; Stepanov, B.S.; Muravyev, S.V. Development of As-Se tapered suspended-core fibers for ultra-broadband mid-IR wavelength conversion. *J. Non-Cryst. Solids* **2018**, *480*, 43–50. [[CrossRef](#)]
28. Coscelli, E.; Poli, F.; Li, J.; Cucinotta, A.; Selli, S. Dispersion Engineering of Highly Nonlinear Chalcogenide Suspended-Core Fibers. *IEEE Photonics J.* **2015**, *7*, 1–8. [[CrossRef](#)]

29. Rodney, W.; Malitson, I.; King, T. Refractive Index of Arsenic Trisulfide. *JOSA* **1958**, *48*, 633–635. [[CrossRef](#)]
30. Knight, J.C.; Birks, T.A.; Russell, P.S.J.; Atkin, D.M. All-silica single-mode optical fiber with photonic crystal cladding: Errata. *Opt. Lett.* **1996**, *21*, 1547–1549. [[CrossRef](#)]
31. Harrington, J.A. *Infrared Fibers and their Applications*; SPIE Press: Bellingham, WS, USA, 2004. [[CrossRef](#)]
32. Chaudhari, C.; Suzuki, T.; Ohishi, Y. Design of Zero Chromatic Dispersion Chalcogenide As S Glass Nanofibers. *IEEE/OSA J. Lightwave Technol. J. Lightwave Technol.* **2009**, *27*, 2095–2099. [[CrossRef](#)]
33. Dudley, J.; Genty, G.; Coen, S. Supercontinuum generation in photonic crystal fiber. *Rev. Mod. Phys.* **2006**, *78*, 1135. [[CrossRef](#)]
34. Xiong, C.; Magi, E.; Luan, F.; Tuniz, A.; Dekker, S.; Sanghera, J.S.; Shaw, L.B.; Aggarwal, I.D.; Eggleton, B.J. Characterization of picosecond pulse nonlinear propagation in chalcogenide As₂S₃ fiber. *Appl. Opt.* **2009**, *48*, 5467–5474. [[CrossRef](#)]
35. Cimpl, Z.; Kosek, F.; Husa, V.; Svoboda, J. Refractive index of arsenic trisulphide. *Czechoslov. J. Phys. B* **1981**, *31*, 1191–1194. [[CrossRef](#)]
36. Yang, T.; Ding, C.; Guo, Y.J. A Highly Birefringent and Nonlinear AsSe₂–As₂S₅ Photonic Crystal Fiber With Two Zero-Dispersion Wavelengths. *IEEE Photonics J.* **2019**, *11*, 1–7. [[CrossRef](#)]
37. Petersen, C.R.; Møller, U.; Kubat, I.; Zhou, B.; Dupont, S.; Ramsay, J.; Benson, T.; Sujecki, S.; Abdel-Moneim, N.; Tang, Z.; et al. Mid-infrared supercontinuum covering the 1.4–13.3 μm molecular fingerprint region using ultra-high NA chalcogenide step-index fibre. *Nat. Photonics* **2014**, *8*, 830–834. [[CrossRef](#)]
38. Du, T.; Li, Y.; Wang, K.; Cai, Z.; Xu, H.; Xu, B.; Mashinsky, V.M.; Luo, Z. 2.01–2.42 μm All-Fiber Femtosecond Raman Soliton Generation in a Heavily Germanium Doped Fiber. *IEEE J. Sel. Top. Quantum Electron.* **2019**, *25*, 1–7. [[CrossRef](#)]
39. Huang, R.; Zhou, R.; Li, Q. Mid-Infrared Supercontinuum Generation in Chalcogenide Photonic Crystal Fibers with a Weak CW Trigger. *J. Lightwave Technol.* **2020**, *38*, 1522–1528. [[CrossRef](#)]
40. Jiao, K.; Yao, J.; Zhao, Z.; Wang, X.; Si, N.; Wang, X.; Chen, P.; Xue, Z.; Tian, Y.; Zhang, B.; et al. Mid-infrared flattened supercontinuum generation in all-normal dispersion tellurium chalcogenide fiber. *Opt. Express* **2019**, *27*, 2036–2043. [[CrossRef](#)]
41. Yang, L.; Li, Y.; Zhang, B.; Wu, T.; Zhao, Y.; Hou, J. 30-W supercontinuum generation based on ZBLAN fiber in an all-fiber configuration. *Photonics Res.* **2019**, *7*, 1061. [[CrossRef](#)]
42. Diouf, M.; Mandeng, L.M.; Tchawoua, C.; Zghal, M. Numerical Investigation of Supercontinuum Generation Through AsSe₂/As₂S₅ Chalcogenide Photonic Crystal Fibres and Rib Structures. *J. Lightwave Technol.* **2019**, *37*, 5692–5698. [[CrossRef](#)]
43. Park, K.; Na, J.; Kim, J.; Jeong, Y. Numerical Study on Supercontinuum Generation in an Active Highly Nonlinear Photonic Crystal Fiber With Anomalous Dispersion. *IEEE J. Quantum Electron.* **2020**, *56*, 1–9. [[CrossRef](#)]

